5 Nano and Materials Science

5-1 Orbital Ordering in a t_{2g} Electron System: MnV_2O_4

Electrons in *d* orbitals often have orbital degrees of freedom – the freedom to occupy different orbitals. Analogously to spin degrees of freedom, orbital degrees of freedom can become ordered at low temperatures (orbital ordering), with particular orbitals occupied at each site. Interestingly, the orbital degree of freedom is often coupled with the spin degree of freedom. This coupling arises from the fact that whether the same orbitals or different orbitals are occupied at neighboring sites is strongly influenced by whether the neighboring spins are aligned in the same direction or in opposite directions.

We have studied single crystals of spinel MnV_2O_4 as a prototypical cubic structure system having orbital degrees of freedom [1, 2]. In this compound, the A site of the spinel structure (AB_2C_4) is occupied by the Mn^{2+} ion, which is in the $3d^5$ high-spin configuration with no orbital degree of freedom, and can be regarded as a simple $S = 5/2$ spin. On the other hand, the B site is occupied by the V^{3+} ion, which takes the $3d^2$ high-spin configuration in the triply degenerate t_{2g} orbital, and has an orbital degree of freedom.

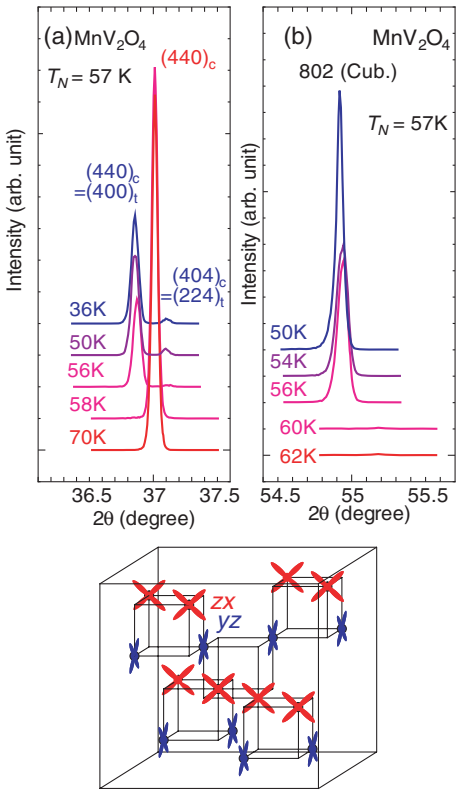

Figure 1
Temperature dependence of (a) the (440) peak and (b) the (802) X-ray diffraction peaks. (c) Schematic diagram of antiferro-orbital ordering in MnV_2O_4.

Figure 1 (a) shows the temperature dependence of the (440) X-ray diffraction peak of a MnV_2O_4 single crystal. The spectra were recorded at BL-4C. The peak sharply splits into two peaks at temperatures below 57 K, indicating a structural phase transition from cubic to tetragonal at this temperature. According to magnetization measurements, ferrimagnetic ordering occurs at the same temperature, indicating simultaneous structural and magnetic phase transitions at 57 K in MnV_2O_4. Figure 1 (b) shows the (802) peak of MnV_2O_4. This peak is forbidden in the cubic spinel structure due to the diamond glide symmetry. However, the peak appears in the tetragonal phase below 57 K, indicating that the diamond glides no longer exist in the tetragonal phase of MnV_2O_4. From this experiment, we can conclude that the antiferro-type ordering of V t_{2g} orbitals, as proposed by Tsunetsugu and Motome [3], where the *yz* and the *zx* orbitals are alternately occupied along the *c* axis as shown in Fig. 1 (c), occurs in the tetragonal phase of MnV_2O_4.

These results show that the spin and orbital degrees of freedom order at the same temperature in MnV_2O_4, and that coupling between them is expected. In order to further study this coupling, X-ray diffraction spectra under an applied magnetic field were recorded at BL-16A1. As shown in Fig. 2 (a), when a magnetic field is applied slightly above the transition temperature, the (800) peak in the cubic phase jumps to that of the tetragonal phase for field strengths above 4 T, indicating a magnetic-field-induced structural phase transition from cubic to tetragonal. On the other hand, when a magnetic

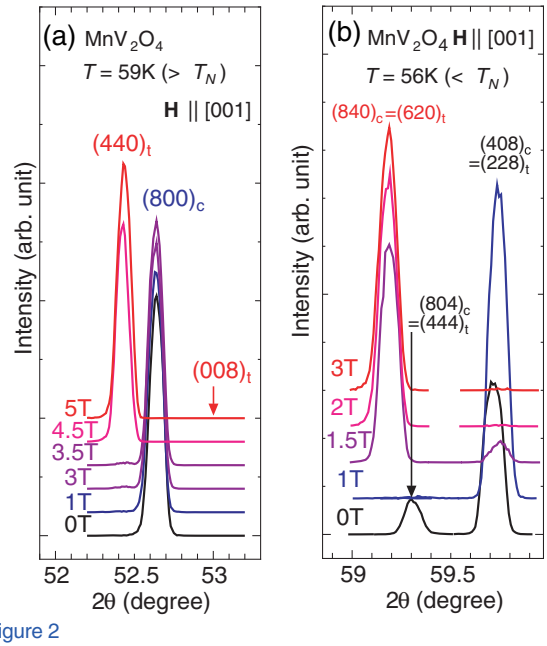

Figure 2
Magnetic-field dependence of (a) the (800) peak at 59 K (above the transition temperature) and (b) the (840) peak at 56 K (below the transition temperature).

field is applied below the transition temperature, the two (840) peaks visible at 0 T merge into a single peak. This indicates that the magnetic field induces an alignment of the crystal domains in the tetragonal phase, with orbital direction being aligned via spin-orbital coupling.

In summary, we have obtained experimental evidence for orbital ordering as well as evidence for the coupling between orbital and spin degrees of freedom in spinel MnV_2O_4 using synchrotron X-ray diffraction measurements on single crystals.

T. Suzuki[1], M. Katsumura[1], K. Taniguchi[2], T. Arima[2] and T. Katsufuji[1] ([1]Waseda Univ., [2]Tohoku Univ.)

References

[1] K. Adachi, T. Suzuki, K. Kato, K. Osaka, M. Takata and T. Katsufuji, *Phys. Rev. Lett.*, **95** (2005) 197202.
[2] T. Suzuki, M. Katsumura, K. Taniguchi, T. Arima and T. Katsufuji, P*hys. Rev. Lett.*, **98** (2007) 127203.
[3] H. Tsunetsugu and Y. Motome, *Phys. Rev. B*, **68** (2003) 060405.

5-2 Orbital-Stripe Rotation and the Charge Polarized State in Double-Layered Manganite

The phenomenon of charge ordering (CO) - the formation of charge stripes - is a central topic in the physics of correlated-electron systems, and is widely observed in transition metal oxides such as layered-structure cuprates [1] and nickelates [2]. Charge ordering in manganites is closely linked to the orbital degrees of freedom of the 3*d* electrons, which leads to staggered orbital ordering (OO) or the formation of orbital stripes. We report here the observation of thermally-induced rotation by 90 degrees of orbital stripes in bilayered manganite crystals with half hole-doping (consisting of a 1:1 ratio of Mn^{3+}/Mn^{4+}) [3, 4]. In addition, the orbital stripe rotation and the consequent CO are found to couple with the underlying lattice distortion to produce a charge-polarized state [5].

The crystal structure of $Pr(Sr_{0.1}Ca_{0.9})_2Mn_2O_7$ was determined from a synchrotron single-crystalline X-ray diffraction pattern recorded using an imaging plate system at BL-1A. As suggested by the two-step anomalies observed in the magnetization (see Fig. 4(a)), there exist two CO-OO phases in this material, which can be associated with the thermally-induced OO rotation. The higher temperature phase is denoted CO1 and the lower temperature one CO2. The diffraction study reveals that the space groups are *Amam* (with a = 5.410, b = 5.462, c = 19.277 Å at 405 K) for the charge disordered phase ($T > T_{CO1}$), *Pbnm* (with a = 5.412, b = 10.921, c = 19.234 Å at 330 K) for the CO1 phase ($T_{CO1} > T > T_{CO2}$), and *Am2m* (with a = 10.812, b = 5.475, c = 19.203 Å at 295 K) for the CO2 phase ($T < T_{CO2}$). Figures 3(a) and (b) show the X-ray oscillation images recorded around the

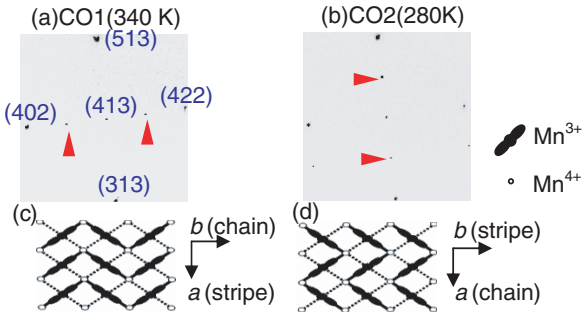

Figure 3
X-ray oscillation images recorded near the 4 1 3 reflection in $Pr(Sr_{0.1}Ca_{0.9})_2Mn_2O_7$ obtained using an imaging plate at (a) 340 K, and (b) 280 K. The red arrows indicate superlattice reflections. Schematic diagrams of the charge and orbital ordering patterns at (c) $T_{CO1} > T > T_{CO2}$ (orbital stripes run along the *a*-axis) and (d) $T < T_{CO2}$ (orbital stripes run along the b-axis) are also shown.

reflection 4 1 3. Because of the formation of charge-orbital stripes, superlattice spots appear at h k±1/2 l (where h, k, l are integers) for the CO1 phase (Fig. 3(a)) and at h±1/2 k l for the CO2 phase (Fig. 3(b)). Note that on the transition from the CO1 to CO2 phase, the superlattice spots move from the *b**-axis to the *a**-axis. This directly reflects a rotation of the orbital stripes by 90 degrees at T_{CO2}, as depicted in Figs. 3(c) and 3(d).

A further interesting aspect of this phenomenon is the emergence of an electrically polar state in the CO2 phase, as anticipated for the space group *Am2m* of the CO2 phase. The insets of Fig. 4(b) illustrate the CO structure of each phase. The crystal structure is orthorhombically distorted even at temperatures above T_{CO1}, *i. e.* each MnO_6 octahedron tilts around the *a*-axis. For the bilayered structure, this distortion causes an alternation in the Mn-O-Mn bond lengths and angles in the MnO_2 plane along the *b*-axis. The structural modulation accompanied by the CO-OO is added to this structure in the lower temperature phases. For simplicity here we take into account only the ordering of the charges, and assume an underlying *Amam* orthorhombic lattice. When the CO transition occurs as shown in Figs. 3(c) and 3(d), the checkerboard pattern of the CO is superimposed onto the bond alternation pattern. This combination of the bond alternation with the CO-induced site alternation induces charge polarization along the *b*-axis in each bilayer. In the CO1 phase, however, the CO pattern stacks to make the inter-bilayer coupling of the polarization antiferroelectric in nature. At T_{CO2}, however, rotation of the orbital stripes is accompanied by rearrangement of Mn^{3+} and Mn^{4+} ions, and the CO stacking pattern is changed as shown in the left-hand insert to Fig. 4. In the CO2 phase, the CO stacks along the *c*-axis so that the polarization of each bilayer along the *b*-axis become additive, forming a *charge-polarized* state below T_{CO2}. This charge polarized state is also confirmed by the observation of a large second harmonic generation susceptibility in the CO2 phase, as depicted in Fig. 4(b).

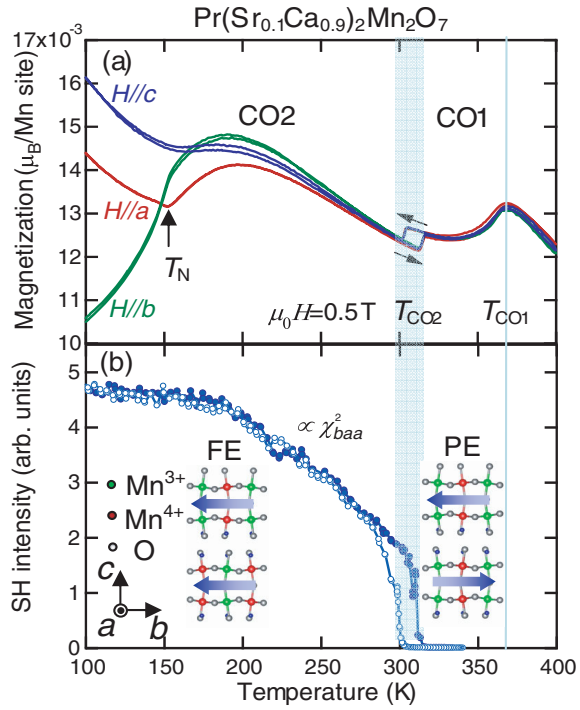

Figure 4
Temperature variation of (a) magnetization in a magnetic field of 0.5 T and (b) second harmonic (SH) light intensity for the tensor component χ^2_{baa}. The insets shows schema of the CO states, with blue arrows indicating possible directions of the dipole moments for the ferroelectric (FE) and paraelectric (PE) cases.

References

[1] J.M. Tranquada, B.J. Sternlieb, J.D. Axe, Y. Nakamura and S. Uchida, *Nature*, **375** (1995) 561.
[2] J.M. Tranquada, D.J. Buttrey, V. Sachan and J.E. Lorenzo, *Phys. Rev. Lett.*, **73** (1994) 1003.
[3] Y. Moritomo, Y. Tomioka, A. Asamitsu, Y. Tokura and Y. Matsui, *Phys. Rev. B*, **51** (1995) 3297.
[4] B.J. Sternlieb, J.P. Hill, Y.C. Wildgruber, G. Luke, B. Nachumi, Y. Moritomo and Y. Tokura, *Phys. Rev. Lett.*, **76** (1996) 2169.
[5] Y. Tokunaga, Th. Lottermoser, Y.S. Lee, R. Kumai, M. Uchida, T. Arima and Y. Tokura, *Nature Mater.*, **5** (2006) 937.

Y. Tokunaga[1,2], R. Kumai[3], Th. Lottermoser[2], T. Arima[2,4] and Y. Tokura[1,2,3,5] ([1]ERATO-MF, [2]ERATO-SSS, [3]CERC-AIST, [4]Tohoku Univ. [5]The Univ. of Tokyo)

5-3 Wigner Crystallization in Molecular Conductor (DI-DCNQI)$_2$Ag

The rarefied electron gas system at high temperature is homogeneous due to the large kinetic energy compared to the Coulomb repulsion among electrons. At extreme low temperatures, the system will tend to condense and make uneven lumps, as theoretically predicted in the early 1930s [1]. Since these lumps carry a negative charge, they form a structure where they try to avoid each other in spatial positioning. We call this phenomenon “Wigner crystallization.”

A molecular conductor (DI-DCNQI)$_2$Ag is insulating even at room temperature and exhibits an antiferromagnetic order at 5.5 K [2]. Planar DI-DCNQI molecules are piled up at even intervals along the *c* direction, composing one-dimensional columns. Since Ag is a monovalent ion having a closed shell, DCNQI molecules have a valence of –1/2 on average and they construct a quarter-filled 1D-π-electron band. Below 220 K, Ref. 3 reported a clear split in the ^{13}C-NMR spectrum and suggested that the $4k_F$ Wigner crystal type of charge order (CO) on DCNQI molecules arose in the low-temperature (LT) phase. This CO ground state on the 1D chain made by long-range Coulomb repulsion was predicted by mean field calculation within the extended Hubbard model [4] in a large *U*/*t* and *V*/*t* region, where *U*, *V* and *t* indicate intra-site, inter-site (intra-chain) interaction and transfer integral, respectively. It is very interesting whether (or how) the electron crystal is stable in the real solid which involves a periodic potential of lattice and an electron-phonon interaction.

Single-crystal X-ray diffraction measurements using synchrotron radiation having a wavelength of 0.6870 Å were performed on a large warped imaging plate camera installed on BL-1A and BL-1B. We tried to analyze the LT structure but were frustrated geometrically in this system. According to several studies [5], the inter-chain Coulomb interaction *V’* is not significantly weak compared to *U* and *V*, and a positive *V’* favors the alternating charge arrangement between the columns. Let us arrange the charge ordered columns to minimize the Coulomb energy. Figure 5 shows a schematic view of columns A, B, C, and B’; the inter-chain interaction *V’* works between two molecules connected by the dashed lines. The valence arrangement in column A is [1: rich, 2: poor], and it determines the valences in B and B’ to be [3: poor, 4: rich] and [3’: poor, 4’: rich]. So far, such arrangement is unique. However, the valence of column C cannot be determined in this manner. Molecule 5 has molecules 3 and 4’ as its relevant neighbors, whose valence is poor and rich, respectively. Molecule 6 has the same condition. We call this situation “spiral frustration”.

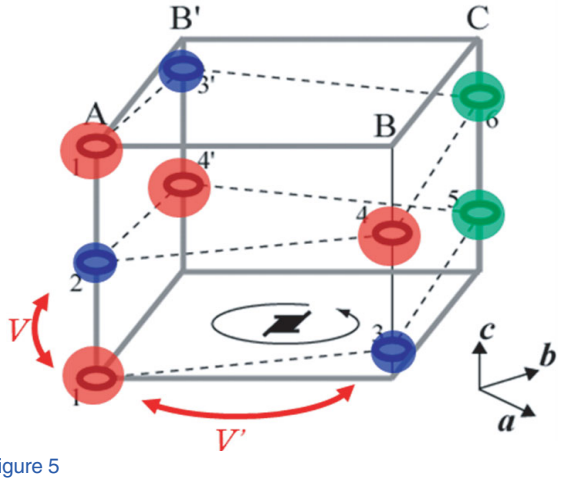

Figure 5
Schematic figure of helical structure along with the A, B, C, and B’ columns. The first neighbor site is on the same chain, and the dashed lines connect second nearest neighbor molecules.

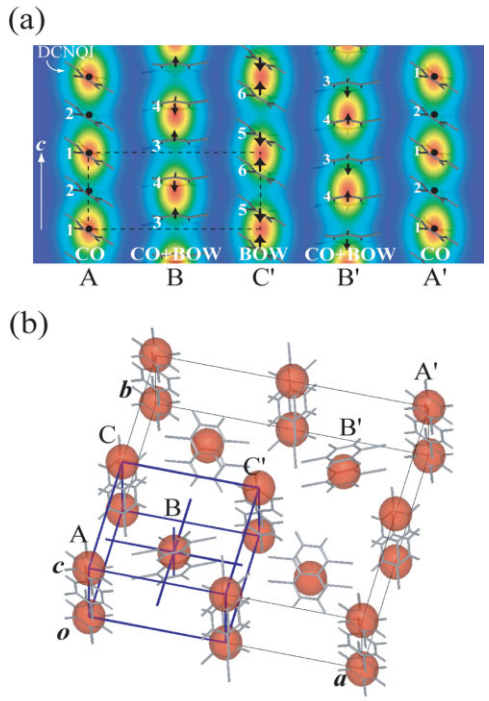

Figure 6
Schematic view of the molecules and charge density waves. (a) Relationship between molecules and charge density waves on each column. Red areas depict electron-rich areas. The arrows show the directions of molecular displacements. (b) Three-dimensional view of the Wigner crystal-type charge arrangement and the molecules. Charge-rich areas are shown by red ellipses, forming a body-centered tetragonal lattice drawn by the blue lines.

Including this frustrated situation, we tried to analyze the LT structure. The result is shown in Fig. 6(a) as schematic charge density wave (CDW). This figure consists of three patterns of charge arrangements: column A shows the CO type, and column C' shows the bond order wave (BOW) type with dimerization of DCNQI molecules. In column B, hybrid states of CO and BOW are established. Figure 6(b) shows the schematic CDW arrangement in the unit cell of the LT phase of $(DI\text{-}DCNQI)_2Ag$, in which the charge-rich areas are depicted by spheres. The charge-rich area forms a body-centered tetragonal lattice with a unit cell of $a_p/2\times b_p/2\times 2c_p$. This charge structure reminds us of the Wigner crystal in which the electrons repel each other. In this system, the origin of the structure is electron-electron interaction and the electron-lattice interaction is negligible, because the CDW phase is not locked to the lattice. Therefore, we conclude that this electronic structure is caused by the Wigner crystallization. [6]

T. Kakiuchi[1], H. Sawa[1], Y. Wakabayashi[1], K. Kanoda[2]
([1]KEK-PF, [2]The Univ. of Tokyo,)

References

[1] E. Wigner, *Phys. Rev.* **46**, 1002 (1934).
[2] K. Hiraki and K. Kanoda, *Phys. Rev. B* **54**, (1996) R17276.
[3] K. Hiraki and K. Kanoda, *Phys. Rev. Lett.* **80**, (1998) 4737.
[4] H. Seo and H. Fukuyama, *J. Phys. Soc. Jpn.* **66**, (1997) 1249.
[5] H. Seo, C. Hotta and H. Fukuyama, *Chem. Rev.* **104**, (2004) 5005, and references therein.
[6] T. Kakiuchi, Y. Wakabayashi, H. Sawa, T. Itou and K. Kanoda, *Phys. Rev. Lett.*, **98** (2007) 066402.

5-4 A Single-Crystal to Single-Crystal Phase Transition under Hydrostatic Conditions Accompanied by a Large Deformation in $Zn(OH)_2$

The study of phase transition mechanisms from the viewpoints of thermodynamics and kinetics is very important for the understanding of first-order phase transitions induced by pressure. It is expected that some of these transitions occur by displacive-type mechanisms. However, this is not easy to prove directly from experimental results since first-order transitions generally occur with polycrystallization, and only limited information on the transition can be obtained [1, 2]. If it were possible to study the phase transition in a pure single crystal under high pressure, it would be possible to discuss the transition mechanism in detail. However, the only such example previously studied is the transition in $CuGeO_3$ [3, 4].

We report here on a phase transition of $Zn(OH)_2$ under hydrostatic conditions. The explorative results [5] suggest that the transition occurs without polycrystallization, a result similar to the case of $CuGeO_3$ [3, 4]. The newly observed phase transition was studied in depth under hydrostatic conditions using both powdered and single crystalline specimens [6]. X-ray powder diffraction patterns were collected using the MAX80 system at AR-NE5C, and the high-pressure behavior of a single crystal was observed using a diamond-anvil cell at Institute for Solid State Physics of the University of Tokyo.

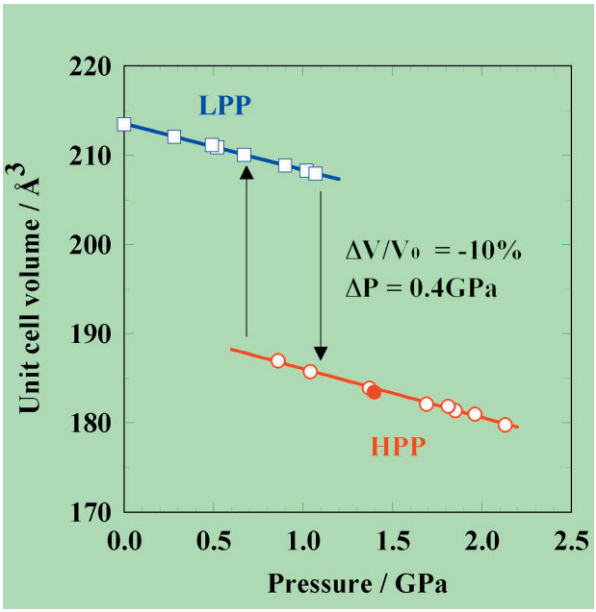

Figure 7
Compression behavior of the low-pressure phase (LPP) and the high-pressure phase (HPP) in $Zn(OH)_2$ under hydrostatic conditions at room temperature. The open and solid symbols indicate data recorded for the powdered and single crystalline specimens, respectively. (This figure was redrawn based on Fig. 8 of Ref. 6 with the permission of Elsevier (16 May 2007.))

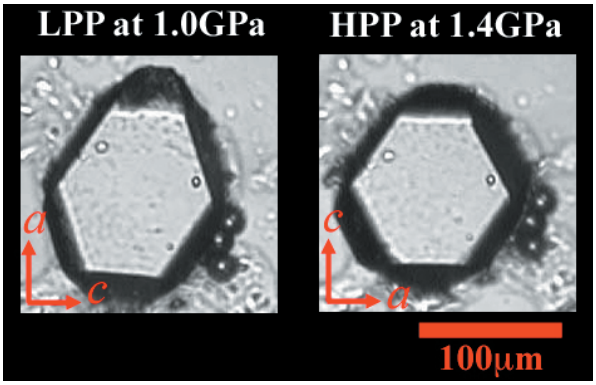

Figure 8
Photomicrographs of a single crystalline specimen in a diamond-anvil cell. The low-pressure phase (LPP) suddenly transformed to the high-pressure phase (HPP) at 1.4 GPa. The crystal orientations were determined from X-ray oscillation photographs. (This figure was redrawn based on Fig. 9 of Ref. 6 with the permission of Elsevier (16 May 2007.))

The X-ray powder diffraction studies [6] revealed that a low-pressure phase (LPP) with an orthorhombic cell structure [7] was stable up to 1.1 GPa, where a sudden transition to a high-pressure phase (HPP) was observed. The HPP was found to have a tetragonal cell structure. The LPP-HPP transition involves a decrease in volume of 10%, as shown in Fig. 7. The HPP reverted to the LPP upon reducing the pressure to around 0.7 GPa: the phase transition is reversible, with a hysteresis of about 0.4 GPa. These two facts clearly indicate a first-order transition.

The shape of the ~100 μm single crystal specimen remained unchanged at pressures below 1.0 GPa, with a sudden change in shape observed at 1.4 GPa, as shown in Fig. 8. It should be noted that no crack was present in the deformed specimen in spite of the large deformation, which occurred within 0.135 seconds. The

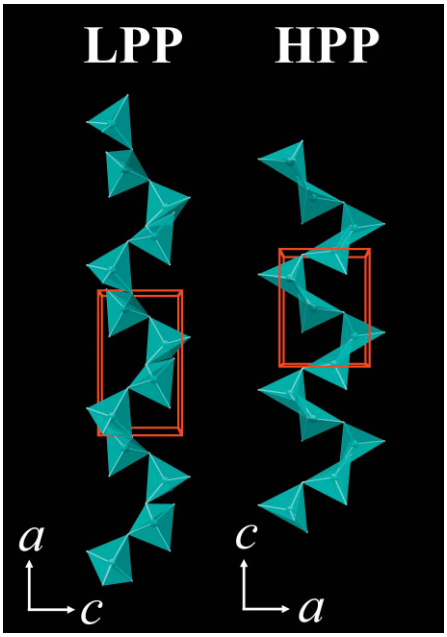

Figure 9
Crystal structures of the low-pressure phase (LPP) with the orthorhombic cell and the high-pressure phase (HPP) with the tetragonal cell. The crystal structure of the HPP was determined from an X-ray oscillation photograph. Hydrogen atoms are ignored.

X-ray reflection pattern recorded using the oscillation photograph method showed that the crystal remained in a tetragonal cell structure, with the same sharpness as that of the LPP, indicating that an LPP-HPP transition occurred and that the HPP specimen remained a single crystal. The crystal-orientation relationships between the orthorhombic LPP and the tetragonal HPP are shown in Fig. 8.

The crystal structures in the LPP and HPP are very similar, as shown in Fig. 9. However a detailed comparison of the helical chains of ZnO_4 tetrahedrons in the two structures reveals a slight difference in the tilt angles of the tetrahedrons. The tilting motion of the tetrahedrons in the transition causes a shortening of the period of the helical chain. In other words, the rotation of ZnO_4 tetrahedrons with no long-range atomic diffusion plays an essential role in the rapid transition, which is accompanied by a large deformation along the *a*-axis of the LPP.

This simple displacive mechanism observed from the microscopic viewpoint is successful in explaining the macroscopic deformation during the transition of the single crystal specimen, and also the kinetic properties of the quick transition. The present results show that the study of this kind of phase transition can provide enough information to understand phase transition mechanisms under high-pressure condition.

K. Kusaba[1], T. Yagi[2], J. Yamaura[2], N. Miyajima[2] and T. Kikegawa[3] ([1]Tohoku Univ., [2]The Univ. of Tokyo, [3]KEK-PF)

References

[1] B. Okai, *J. Phys. Soc. Jpn.*, **48** (1980) 514.
[2] A. Onodera, Y. Nakai, S. Kawano and N. Achiwa, *High Temp. High Press.*, **24** (1992) 55.
[3] A. Jayaraman, S.Y. Wang and L.C. Ming, *Phys. Rev. Lett.*, **75** (1995) 2356.
[4] A. Yoshiasa, G. Yagyu, T. Ito, T. Yamanaka and T. Nagai, *Z. Anorg. Allg. Chem.*, **626** (2000) 36.
[5] K. Kusaba and T. Kikegawa, *PF Act. Rep.*, **21B** (2004) 200.
[6] K. Kusaba, T. Yagi, J. Yamaura, N. Miyajima and T. Kikegawa, *Chem. Phys. Lett.*, **437** (2007) 61.
[7] R.W. G. Wyckoff, *Crystal Structures 2nd ed.*, **1**, (Robert E. Krieger Publishing, Malabar, 1982).

5-5 Unusual Crystallization Behaviors from a Molecularly Thin Nanosheet Reactant

Nucleation and crystal growth from various reactants have been widely studied in the past few decades in the quest to achieve fine control of crystallization and thus design a range of functional materials. Due to the recent development of material design using nanomaterials, novel reactant systems may be precisely fabricated. These include two-dimensional solid systems which have thicknesses on the molecular range, that is believed to severely hinder nucleation and crystal growth.

Study of such systems may provide knowledge on thickness effects for crystallization behavior.

Here we report interesting crystallization behaviors of anatase nanocrystallites in a molecularly thin reactant composed of exfoliated titania nanosheets [1]. The heating process of the well-organized films allowed the film thickness to be accurately controlled, varying from single monolayer to stacked multilayer with a stepwise increment of ~1 nm. The process was monitored using X-ray absorption near edge structure (XANES) analysis under the total reflection fluorescence (TRF) mode, along with in-plane X-ray diffraction (XRD) measurements using a synchrotron radiation source.

A colloidal suspension of the titania nanosheets with composition $Ti_{0.87}O_2$ was obtained by delaminating a layered titanate into single host layers [2]. The resulting unilamellar crystallites were deposited onto quartz and Si substrates into highly organized monolayer and multilayer (2, 3, 5, 10 layers) films by electrostatic self-assembly and subsequent ultrasonic treatment. The films were heated to 300, 400, 500, 600, 700, 800 and 900°C for 1 h in air, and measurements were carried out at BL-12C (TRF-XANES) and BL-6C (XRD) to characterize the crystallization behavior of the nanosheets. Figure 10 shows in-plane diffraction patterns of the monolayer and multilayer films before and after anatase crystallization. The as-grown nanosheet exhibits three diffraction peaks at 4.28, 5.31 and 6.73 nm^{-1}, which are indexable to 11, 20 and 02 of its 2-dimensional (2D) rectangular unit cell, in the 1/d region from 4 nm^{-1} to 7 nm^{-1}. Upon heating the monolayer film to 800°C, the 20 peak shifted slightly to a smaller 1/d value. Heating further to 900°C shifted

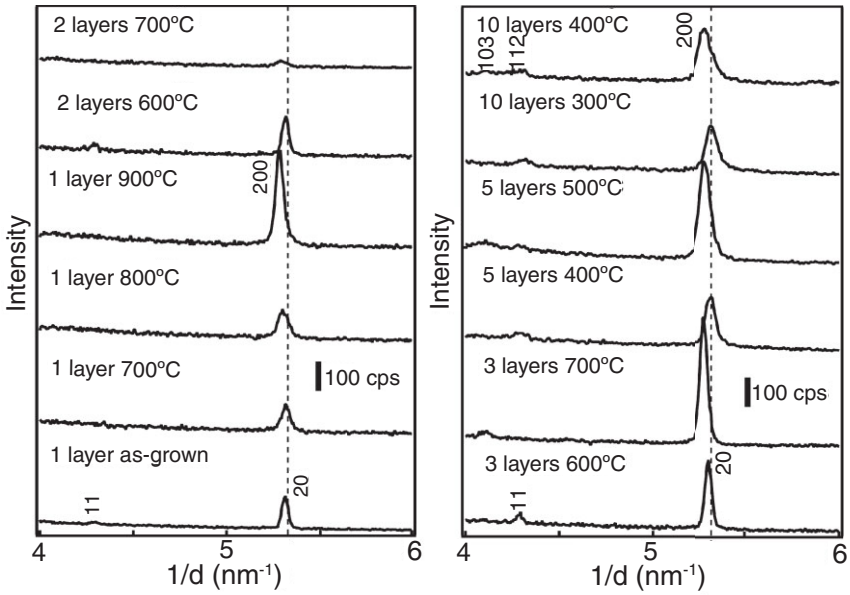

Figure 10
In-plane diffraction patterns of the nanosheet films with layer numbers of 1, 2, 3, 5 and 10 before and after heating at the crystallization temperature of anatase.

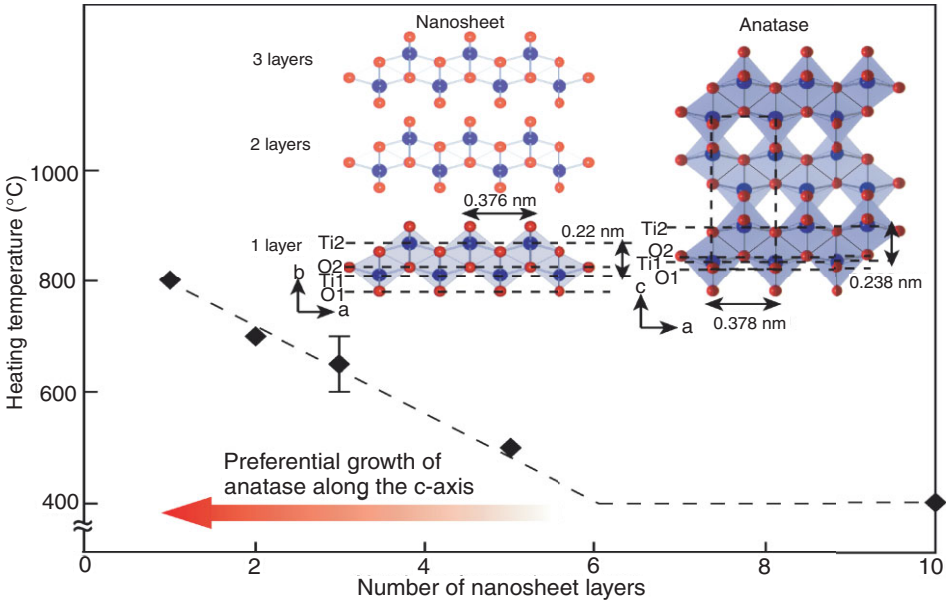

Figure 11
Layer number dependence of the crystallization temperature for anatase. The inset shows the atomic architectures of the titania nanosheet and anatase, with Ti atoms shown in blue and O atoms in red.

the peak to 5.28 nm^{-1}, assignable to the 200 reflection of anatase. This shift can be employed as an indicator to identify transformation from the nanosheet to anatase even in the thicker films. The films with 5 and 10 nanosheet layers were transformed into anatase at 400 – 500°C, a temperature similar to the common crystallization temperature of anatase from bulk reactants [3]. For thinner films with less than 5 nanosheet layers the crystallization temperature gradually increases, reaching 800°C for the monolayer film. The TRF-XANES monitoring also supported this thickness-dependent change in the crystallization temperature (results not shown). The crystallization temperature estimated in this work is plotted against layer number in Fig. 11. Interestingly, anatase transformed from the ultrathin films with only 1 or 2 nanosheet layers exhibited only the 200 peak, indicating preferential growth of anatase along the *c*-axis.

This unusual thermal behavior may be understood in terms of crystallization from the 2D system of scarcely distributed reactants. The titania nanosheet crystallite is much thinner than the unit cell dimensions of anatase, as shown in Fig. 11. Extensive atomic diffusion is therefore required for crystallization, particularly for ultrathin films with small numbers of nanosheet layers. This so-called diffusion-rate limiting process should bring about the preferential growth of anatase based on the structural similarity between anatase and titania nanosheet. Further details are described in a separate publication [1].

K. Fukuda[1], Y. Ebina[1], I. Nakai[2] and T. Sasaki[1] ([1]NIMS, [2]Tokyo Univ. of Sci.)

References

[1] K. Fukuda, Y. Ebina, T. Shibata, T. Aizawa, I. Nakai and T. Sasaki, *J. Am. Chem. Soc.*, **129** (2007) 202.
[2] T. Tanaka, Y. Ebina, K. Takada, K. Kurashima and T. Sasaki, *Chem. Mater.*, **15** (2003) 3564.
[3] T. Sasaki, M. Watanabe, Y. Michiue, Y. Komatsu, F. Izumi and S. Takenouchi, *Chem. Mater.*, **7** (1995) 1001.